


Resonant-driving-induced ferromagnetism in the Fermi-Hubbard model

Ning Sun, Pengfei Zhang, and Hui Zhai

Institute for Advanced Study, Tsinghua University, Beijing 100084, China

 (Received 20 September 2018; revised manuscript received 21 November 2018; published 29 April 2019)

In this article we study quantum phases and the phase diagram of a Fermi-Hubbard model under periodic driving that has been realized in recent cold-atom experiments, in particular, when the driving frequency is nearly resonant with the interaction energy. Due to the driving, the effective Hamiltonian contains a correlated hopping term where the density occupation strongly modifies the hopping strength. Focusing on half filling, in addition to the charge- and spin-density wave phases, large regions of ferromagnetic phase and phase separation are discovered in the weakly interacting regime. The mechanism of this ferromagnetism is attributed to the correlated hopping, because the hopping strength within a ferromagnetic domain is normalized to a larger value than the hopping strength across the domain. Thus, the kinetic energy drives the system into a ferromagnetic phase. We note that this is a different mechanism, in contrast to the well-known Stoner mechanism for ferromagnetism where the ferromagnetism is driven by interaction energy.

DOI: [10.1103/PhysRevA.99.043629](https://doi.org/10.1103/PhysRevA.99.043629)

Recently, tremendous experimental progress has been made on quantum simulation of the Fermi-Hubbard model [1–17], including the observation of equilibrium properties such as short-range antiferromagnetic correlations [7–9], hidden antiferromagnetic correlations [10], incommensurate spin correlations [11], canted antiferromagnetic correlations [12], and pairing correlations [13]. In particular, antiferromagnetic quasi-long-range order has been successfully observed through entropy engineering [14]. Recent advances also include nonequilibrium behaviors such as the measurement of optical conductivity [15] and the spin- and charge-transport coefficients [16,17].

Studying the Fermi-Hubbard model with cold atoms also allows us to open up a new avenue beyond the traditional condensed-matter paradigm. One example is the periodically driven Fermi-Hubbard model [18,19]. Since the typical parameters of a Hubbard model are the hopping strength J and the on-site interaction U , both of which are of the order of electronvolt in strongly correlated solid-state materials, it is therefore hard to drive a solid-state material with frequency resonant with any of these two energy scales. However, in a cold-atom realization of the Fermi-Hubbard model, the typical energy scales for these two parameters are both of the order of hundreds to thousands of Hertz, and it is quite easy to drive the optical lattices with such a frequency. When the driving frequency is nearly resonant with the interaction parameter U , the driving can strongly modify the Fermi-Hubbard model, as observed in recent experiments [20,21]. Hence, it is very promising to study novel physics induced by periodic driving that cannot be accessed in a static system. The goal of this paper is therefore to predict the quantum phases and phase diagram of the nearly resonant-driven Fermi-Hubbard model that is newly realized in cold-atom experiments.

Model. We consider a two-dimensional square lattice (see Fig. 1) periodically modulated along the \hat{x} and \hat{y} directions with a frequency ω and an amplitude A whose single-particle

Hamiltonian can be written as

$$\hat{H}_0(t) = \frac{\mathbf{p}^2}{2m} + \hat{V}[x + A \cos(\omega t), y + A \cos(\omega t)], \quad (1)$$

where m is the mass of an atom. We can now perform a unitary transformation [22]

$$\hat{U}(t) = \exp[i\mathbf{p} \cdot \mathbf{r}_0(t)/\hbar], \quad (2)$$

where $\mathbf{r}_0(t) = -A \cos(\omega t)(1, 1)$ are two-dimensional vectors. This unitary transformation transfers position $\mathbf{r}_0(t)$ into the comoving frame with an extra time-dependent gauge field introduced. The resulting Hamiltonian is written as

$$\hat{H}_0(t) = \frac{(\mathbf{p} - \mathbf{A}(t))^2}{2m} + \hat{V}(\mathbf{r}), \quad (3)$$

with $\mathbf{A}(t) = m\mathbf{r}'_0(t)$. The Hamiltonian Eq. (3) is equivalent to Eq. (1) but more convenient for the later purpose.

Utilizing the Peierls substitution, the single-band Hamiltonian in a second quantized form can be written as

$$\begin{aligned} \hat{H}(t) = & -J \sum_{\substack{\langle i, j \rangle \\ \sigma = \uparrow, \downarrow}} e^{i\mathbf{d}_{ij} \cdot \mathbf{A}(t)/\hbar} \hat{c}_{i\sigma}^\dagger \hat{c}_{j\sigma} \\ & + U \sum_i \left(\hat{n}_{i\uparrow} - \frac{1}{2} \right) \left(\hat{n}_{i\downarrow} - \frac{1}{2} \right), \end{aligned} \quad (4)$$

where $\hat{c}_{i\sigma}$ ($\hat{c}_{i\sigma}^\dagger$) is the fermionic annihilation (creation) operator on site i with spin σ , $\hat{n}_{i\sigma}$ is the density operator on site i with spin σ , $\langle \dots \rangle$ denotes the nearest-neighboring sites, and $\mathbf{d}_{ij} = \mathbf{d}_i - \mathbf{d}_j$, with \mathbf{d}_i being the position of the i th lattice site. Throughout this work we focus on the half-filling case and the chemical potential is set to zero.

When the modulation frequency ω is the largest energy scale of the problem, that is to say, it is much larger than both the interaction parameter U and the hopping J , one can do a high-frequency expansion and truncate to the lowest order to obtain an effective time-independent Hamiltonian [23,24].

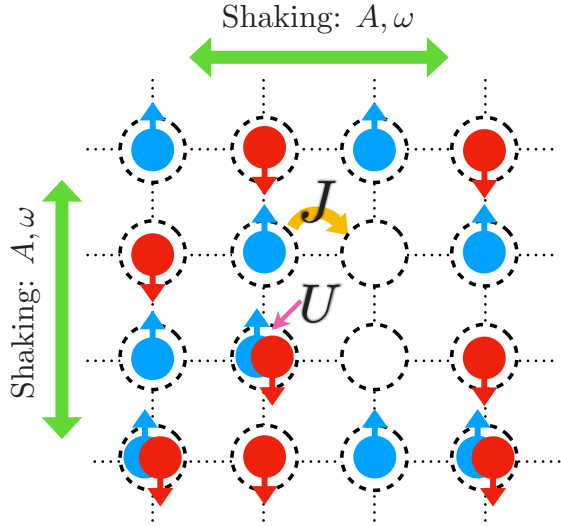


FIG. 1. A schematic of the Fermi-Hubbard model on a two-dimensional square lattice. Arrows indicate the direction of shaking. Balls with different colors and arrows indicate fermions with different spins.

The effective Hamiltonian takes the same form as a normal Hubbard model, with the only modification that the tunneling coefficient being renormalized by the oscillating gauge field is $\tilde{J} = J\mathcal{B}_l(\mathcal{A})$, where we use \mathcal{B}_l to denote the l th Bessel function and $\mathcal{A} = m\omega d/\hbar$ the normalized shaking amplitude. d is the distance of two Wannier wave packets in the nearest-neighbor lattice sites.

However, this expansion fails when the modulation frequency ω , or l th multiple of it, is comparable to one of the energy scales of the problem, say, the interaction strength U , for which case we call it the l th resonance. In this case, since U is no longer very small compared with ω while $U - l\hbar\omega$ is a much smaller energy scale, we apply another unitary transformation,

$$\hat{R}(t) = \exp\left(i \sum_j l\omega t \hat{n}_{j\uparrow} \hat{n}_{j\downarrow}\right), \quad (5)$$

that alters the interaction strength to an effective one $\tilde{U} = U - l\hbar\omega$. Now $\tilde{U} \sim J \ll U \sim l\hbar\omega$. Moreover, since $\hat{R}(t)$ does not commute with the Hamiltonian, it introduces an additional density dependence to the hopping term and effectively alters the gauge field into a spin- and density-dependent one as follows:

$$\tilde{\mathbf{A}}_{ij,\sigma}(t) = \mathbf{A}(t) - \frac{l\omega t}{d^2} \mathbf{d}_{ij} [(1 - \hat{n}_{i\bar{\sigma}}) \hat{n}_{j\bar{\sigma}} - (1 - \hat{n}_{j\bar{\sigma}}) \hat{n}_{i\bar{\sigma}}]. \quad (6)$$

Now the high-frequency expansion can be safely done, and to the lowest order it again results in a time-independent effective Hamiltonian written as

$$\hat{H}_{\text{eff}} = \sum_{(i,j),\sigma} -\tilde{f}_{\text{eff},\sigma}^{(ij)} \hat{c}_{i\sigma}^\dagger \hat{c}_{j\sigma} + \tilde{U} \sum_i \left(\hat{n}_{i\uparrow} - \frac{1}{2}\right) \left(\hat{n}_{i\downarrow} - \frac{1}{2}\right). \quad (7)$$

Here $\tilde{f}_{\text{eff},\sigma}^{(ij)}$ is introduced as

$$\tilde{f}_{\text{eff},\sigma}^{(ij)} = J_0 \hat{a}_{ij\bar{\sigma}} + J_1 \hat{b}_{ij\bar{\sigma}}, \quad (8)$$

where $\bar{\sigma}$ denotes the complement of σ , $J_0 = J\mathcal{B}_0(\mathcal{A})$, $J_1 = J\mathcal{B}_l(\eta_{ij}\mathcal{A})$ [$\eta_{ij} = \pm 1$ for $(i_x, i_y) = (j_x \pm 1, j_y)$ or $(i_x, i_y) = (j_x, j_y \pm 1)$], and

$$\hat{a}_{ij\sigma} = (1 - \hat{n}_{i\sigma})(1 - \hat{n}_{j\sigma}) + \hat{n}_{i\sigma} \hat{n}_{j\sigma}, \quad (9)$$

$$\hat{b}_{ij\sigma} = (-1)^l (1 - \hat{n}_{i\sigma}) \hat{n}_{j\sigma} + \hat{n}_{i\sigma} (1 - \hat{n}_{j\sigma}). \quad (10)$$

In the above, the site dependence of J_1 is made implicit. Note, however, that for even l the Bessel function \mathcal{B}_l is an even function, in which case η_{ij} can be simply dropped and J_1 becomes a constant. In contrast to the off-resonance case, now the hopping strength depends on the site occupation of fermions. As we will show below, this correlated hopping plays a key role in the emergent new mechanism for the ferromagnetism phase.

Symmetry. Before we delve into solving this effective Hamiltonian, let us first comment on the symmetry of this problem. Note that the original Hubbard model possesses a SO(4) symmetry [25], which is composed of a spin SU(2), generated by $\hat{S}_z = (1/2) \sum_i \hat{c}_{i\uparrow}^\dagger \hat{c}_{i\uparrow} - \hat{c}_{i\downarrow}^\dagger \hat{c}_{i\downarrow}$, $\hat{S}_+ = \sum_i \hat{c}_{i\uparrow}^\dagger \hat{c}_{i\downarrow}$, and $\hat{S}_- = \hat{S}_+^\dagger$, and a charge SU(2), generated by $\hat{L}_z = -(1/2) \sum_i \hat{c}_{i\uparrow}^\dagger \hat{c}_{i\uparrow} + \hat{c}_{i\downarrow}^\dagger \hat{c}_{i\downarrow} + N_s/2$, $\hat{L}_+ = \sum_i (-1)^i \hat{c}_{i\uparrow}^\dagger \hat{c}_{i\downarrow}$, and $\hat{L}_- = \hat{L}_+^\dagger$. N_s is the total number of sites. The spin SU(2) ensures that the direction of the spin-density-wave (SDW) order parameter can be taken along any direction, and the charge SU(2) ensures the degeneracy of a charge-density-wave (CDW) order and the fermion pairing order (P).

Considering the time-dependent Hamiltonian Eq. (4), it is straightforward to show that the spin SU(2) symmetry stays, yet the charge SU(2) symmetry no longer holds since L_\pm do not commute with the kinetic term. However, considering the time-independent effective Hamiltonian Eq. (7), one can show that the charge SU(2) symmetry is recovered for the even- l case although not for the odd- l case [26]. Hereafter we focus only on the even- l case, which possesses the same SO(4) symmetry. In addition, it also possesses the particle-hole symmetry at half filling.

Phase diagram. We present our results on the phase diagram derived from a standard mean-field treatment on this effective Hamiltonian Eq. (7), which is known to be qualitatively reliable for a normal Hubbard model on a square lattice at half filling (the dot-dashed green line on Fig. 2) because the ordering occurs with an infinitesimal weak interaction parameter due to the nesting effect [26,27]. Thanks to the SO(4) symmetry, we can choose SDW along \hat{z} direction (i.e., $s_i = \langle \hat{n}_{i\uparrow} - \hat{n}_{i\downarrow} \rangle$) and CDW (i.e., $c_i = \langle \hat{n}_{i\uparrow} + \hat{n}_{i\downarrow} \rangle - 1$) as the order parameters in our mean-field theory. A higher-order effect will break the degeneracy between CDW and P, but it is beyond the scope of current work.

The phase diagram is shown in Fig. 2, which is controlled by two parameters of J_1/J_0 and $\tilde{U}/|J_0|$. As a benchmark of our calculation, first of all, when $J_1/J_0 = 1$, because of $\hat{a}_{ij\sigma} + \hat{b}_{ij\sigma} = \hat{I}$, the kinetic energy term becomes $-J_0 \sum_{(ij),\sigma} \hat{c}_{i\sigma}^\dagger \hat{c}_{j\sigma}$ and the Hamiltonian recovers the usual Hubbard model. In this case (labeled by 2 and the underlying dot-dashed green

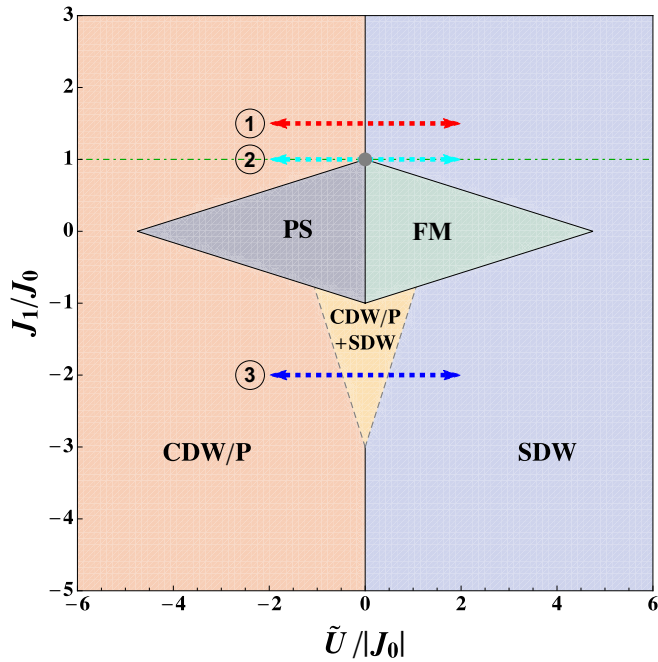


FIG. 2. Phase diagram for the effective Hamiltonian Eq. (7) of a nearly resonant-driven Fermi-Hubbard model with even l at half filling. The phase diagram is controlled by two dimensionless parameters, J_1/J_0 and $\tilde{U}/|J_0|$. “CDW” and “SDW” denote charge- and spin-density wave order. “P” denotes fermion pairing order. “FM” denotes ferromagnetism. “PS” denotes phase separation into high- and low-density regimes. Solid lines are a first-order phase transition, and the dashed lines denote the second-order phase transition. Dashed arrows mark the lines along which the order parameters are plotted in Fig. 3.

line in Fig. 2), the result for the normal Hubbard model is retrieved where we obtain a CDW order of (π, π) with attractive interaction ($\tilde{U} < 0$) and a SDW order of (π, π) with repulsive interaction ($\tilde{U} > 0$). Explicitly, the order parameters are chosen as $s_i = (-1)^{i_x+i_y}s$ and $c_i = (-1)^{i_x+i_y}c$, and $s(c)$ gradually vanishes as \tilde{U} approaches zero from the positive (negative) side. As a result, a second-order phase transition occurs at $\tilde{U} = 0$ (gray dot in Fig. 2). This can be seen from the order parameters plotted as a function of $\tilde{U}/|J_0|$, shown as cyan (lower) curves in Fig. 3.

Since both CDW and SDW are ordered phases, it should be either a first-order transition or a phase coexistence regime in between for more generic situations. As marked by the solid vertical lines in Fig. 2, it is a first-order transition on the phase boundary at large $|J_1/J_0|$. The magnitude of order parameters is shown with red (middle) lines in Fig. 3 (labeled by 1 in Fig. 2) that jump from a finite value to zero at $\tilde{U} \rightarrow 0$. In between, a CDW and SDW coexistence regime shows up at a certain range of J_1/J_0 , as displayed by the yellow region in Fig. 2, whose order parameters are shown with blue (upper) lines in Fig. 3 for a representative case (labeled by 3 in Fig. 2).

The most notable feature in Fig. 2 is the middle green and dark-gray region. In this region a mean-field ansatz of CDW or SDW orders with ordering vector at (π, π) may not yield any ordered solution. However, when we consider the case of enlarged 2×2 , 3×3 , up to $L \times L$ domains, and within each domain the CDW and SDW order parameters are uniformly

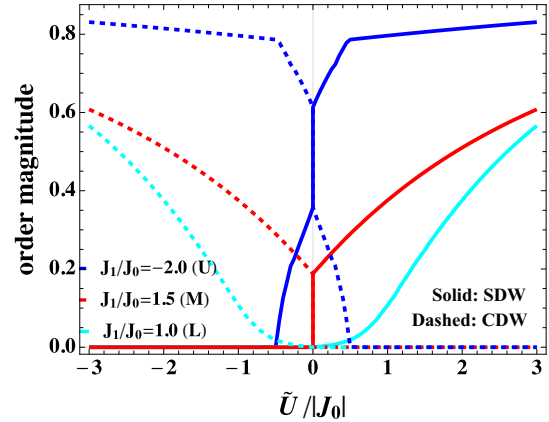


FIG. 3. The CDW order parameter c (dashed lines) and the SDW order parameter s (solid lines) as a function of $\tilde{U}/|J_0|$ for three representative cases labeled 1–3 in Fig. 2, with $J_1/J_0 = 1.5$ (middle line, M), 1.0 (lower line, L), and -2.0 (upper line, U), respectively.

chosen as c and s while in its neighboring domain they are taken as $-c$ and $-s$, the mean-field ansatz does yield ordered solutions. It can be seen from Fig. 4 that the mean-field ground-state energy decreases monotonically as L increases, indicating that the ground state will form large domains with opposite order-parameter values. Moreover, minimizing the ground-state energy yields $c = 0$ and $s \neq 0$ at positive \tilde{U} and $c \neq 0$ and $s = 0$ at negative \tilde{U} . Hence, the system with positive \tilde{U} possesses spin order, and the increase of the domain size indicates the decrease of the spin-ordering wave vector. Eventually, the wave vector decreases toward zero, and the ground state becomes a ferromagnetic state. In other words, as the domain size becomes larger and larger, the system is essentially made of ferromagnetic domains. For negative \tilde{U} the system tends toward phase separation, with high density in one domain and low density in its neighboring domains.

It should be emphasized that both the ferromagnetism and the phase separation regime can occur at small \tilde{U} . In fact, this is purely due to the correlated hopping effect in the

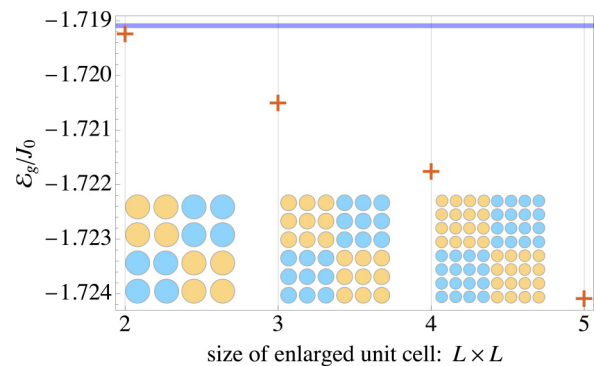


FIG. 4. The mean-field ground-state energy (ϵ_g) as a function of the domain size L for a representative case $J_1 = 0$, $\tilde{U}/|J_0| = -0.2$. The insets show the configuration for 2×2 , 3×3 , and 4×4 blocks where the CDW and SDW order parameters are uniformly distributed within a domain and take opposite values between neighboring domains. For comparison, the solid line is the mean-field energy when order parameters are all zero.

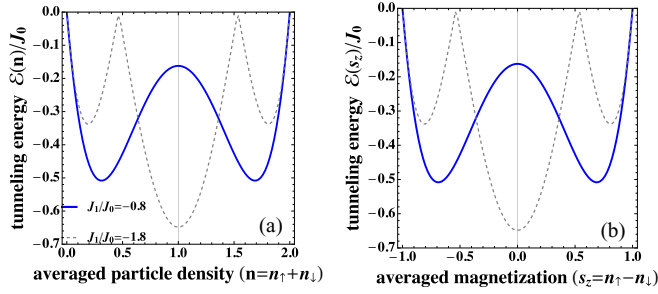


FIG. 5. The mean-field energy with $\tilde{U} = 0$ (a) as a function of total density n with $s_z = 0$ fixed and (b) as a function of s_z with $n = 1$ fixed. Solid line is for the PS/FM case ($J_1/J_0 = -0.8$), and the dashed line is for the coexistence case ($J_1/J_0 = -1.8$).

effective Hamiltonian Eq. (7), which originates essentially from the nearly resonant driving. Considering the mean-field configurations as shown in the insets of Fig. 4, let us look at the mean-field value of the effective hopping strength $\langle \hat{J}_{\text{eff},\sigma}^{(ij)} \rangle$, which quantifies how the particle occupation affects the hopping strength. We define $J_{\text{eff},\sigma}^{\text{intra}}$ as $\langle \hat{J}_{\text{eff},\sigma}^{(ij)} \rangle$, with i and j in the same domain, and $J_{\text{eff},\sigma}^{\text{inter}}$ as $\langle \hat{J}_{\text{eff},\sigma}^{(ij)} \rangle$, with i and j across two neighboring domains. It is straightforward to write $J_{\text{eff},\sigma}^{\text{intra}}$ and $J_{\text{eff},\sigma}^{\text{inter}}$, respectively, as

$$J_{\text{eff},\sigma}^{\text{intra}} = \frac{1}{2}(J_0[1 + (c \mp s)^2] + J_1[1 - (c \mp s)^2]), \quad (11)$$

$$J_{\text{eff},\sigma}^{\text{inter}} = \frac{1}{2}(J_0[1 - (c \mp s)^2] + J_1[1 + (c \mp s)^2]), \quad (12)$$

where \mp corresponds to different spin components. One can show that when $|J_1| < |J_0|$, $|J_{\text{eff},\sigma}^{\text{inter}}|$ is always smaller than $|J_{\text{eff},\sigma}^{\text{intra}}|$. Hence, the size of the domain tends to increase such that there are more intradomain links than interdomain links, and therefore the effective bandwidth becomes larger. For a given filling, a larger bandwidth leads to more kinetic energy gain. $|J_1| < |J_0|$ is precisely the regime where we find ferromagnetism or phase separation in the phase diagram of Fig. 3 with arbitrary weak interaction. This regime can be easily accessed when \mathcal{A} is small by exploring a small shaking amplitude.

An alternative way to understand the emergence of this ferromagnetism is to consider a uniform system with $\tilde{U} = 0$. Substituting $\hat{J}_{\text{eff},\sigma}^{(ij)}$ by its mean-field value, it is straightforward to compute the kinetic energy of this uniform system that depends on n_{\uparrow} and n_{\downarrow} , where $n_{\uparrow} = (n + s_z)/2$ and $n_{\downarrow} = (n - s_z)/2$. We plot the kinetic energy as a function of n with $s_z = 0$ in Fig. 5(a) and as a function of s_z with $n = 1$ in Fig. 5(b) for two representative cases of $J_1/J_0 = -0.8$ and -1.8 . One can see from Fig. 5(a) that for $J_1/J_0 = -0.8$, there are two local minima, with one at $n > 1$ and the other at $n < 1$, who are located symmetrically on two sides of $n = 1$, while for $J_1/J_0 = -1.8$ there is only one minimum located at $n = 1$. Similarly, in Fig. 5(b) for $J_1/J_0 = -0.8$ there are two local minima with one at positive s_z and the other at negative s_z , symmetrically distributed around $s_z = 0$, and for $J_1/J_0 = -1.8$ there is only one minimum at $s_z = 0$. Thus, when the system is constrained with the average $n = 1$ and $s_z = 0$, for the case with $J_1/J_0 = -0.8$, it will actually phase

separate into domains with either different n or different s_z , corresponding to either phase separation or ferromagnetism, respectively. The choice is made by the sign of \tilde{U} when a small but finite \tilde{U} perturbation is turned on.

Conclusion and discussion. In contrast to the well-known Stoner mechanism for ferromagnetism driven by the interaction energy, the most significant finding of this work is to provide an alternative mechanism for the onset of ferromagnetism which roots in the cooperation between the spin order and the correlated hopping. This is also different from the ferromagnetism due to the superexchange processes discussed in the experiment of Ref. [20] which requires \tilde{U} to be negative.

We also note that in previous literature, there are a number of works which have studied the same or similar density-assisted hopping models in one dimension [28–36]. However, none of these papers discovers the ferromagnetic state predicted here. In [28], their method works only for sufficiently large \tilde{U} . In [29–31], the authors find that the ground state at half filling can be explained by phase separation for charge, but the ferromagnetism is not discussed. In [32], the quantum Monte Carlo they used does not converge for small J_1 . The works using the bosonization method assume a uniform background, for which they overlook the possibility of ferromagnetism [33–35]. An exact diagonalization calculation with a small number of sites also may not be able to capture such physics [36].

Finally, we shall comment on the experimental observation of this ferromagnetism. First of all, the ETH group has realized a resonantly shaking honeycomb lattice with cold Fermi gases where the heating takes over only after a relatively long time scale [20,37]. Second, it requires a moderate interaction parameter U , because, on one hand, U is comparable with $\hbar\omega$ and has to be much larger than the bandwidth $\sim J$, and on the other hand, U has to be smaller than the band gap in order to allow the single-band model to be valid, i.e., $\hbar\omega \sim U < \frac{\hbar^2}{md^2}$. This leads to $\mathcal{A} = m\omega Ad/\hbar < A/d$. For small shaking amplitude $A/d < 1$, we then have small \mathcal{A} where $J_0 > J_1 > 0$. In such a parameter regime, we should be able to observe the ferromagnetism. Third, because this ferromagnetism is driven by the kinetic energy, one expects that this ferromagnetism can be observed when temperature is of the order of the bandwidth, which can be accessed now by cold-atom experiments where $T/T_F \sim 0.1$ [20]. Finally, the quantum gas microscope techniques can be used to detect real-space ferromagnetic domains. Hence, it is quite promising to expect experimental verification of the theoretic expectations discussed here in the very near future.

Acknowledgments. This work is supported by MOST under Grant No. 2016YFA0301600 and the NSFC through Grant No. 11734010.

APPENDIX A: SYMMETRY

In this section we discuss the symmetry of the resonantly driven Fermi-Hubbard model. The symmetry is of vital significance, since it greatly simplifies the formulation of the mean-field description.

SO(4) symmetry. A usual bipartite Fermi-Hubbard model, written as $\hat{H} = -J \sum_{(i,j),\sigma} \hat{c}_{i\sigma}^\dagger \hat{c}_{j\sigma} + \tilde{U} \sum_i (\hat{n}_{i\uparrow} - 1/2)(\hat{n}_{i\downarrow} - 1/2)$, possesses SO(4) symmetry [25]. The SO(4) symmetry is resolved into two SU(2) symmetries—the spin SU(2) and the charge SU(2). The generators of spin SU(2) are given by

$$\hat{S}_z = \frac{1}{2} \sum_i \hat{c}_{i\uparrow}^\dagger \hat{c}_{i\uparrow} - \hat{c}_{i\downarrow} \hat{c}_{i\downarrow}, \quad \hat{S}_+ = \sum_i \hat{c}_{i\uparrow}^\dagger \hat{c}_{i\downarrow} \quad (\text{A1})$$

and

$$\hat{S}_- = \hat{S}_+^\dagger, \quad \hat{S}_x = \frac{\hat{S}_+ + \hat{S}_-}{2}, \quad \hat{S}_y = \frac{\hat{S}_+ - \hat{S}_-}{2i}, \quad (\text{A2})$$

which satisfy the commutation relation of the SU(2) algebra. Due to the contraction between spin indices, the very beginning time-dependent Hamiltonian $\hat{H}(t)$ [Eq. (4) in the main text] is invariant under these SU(2) symmetry operations and also the unitary transformations $\hat{R}(t)$ [Eqs. (5) and (6) in the main text]. Since the time average does not alter this attribute, one arrives at the conclusion that the effective static Hamiltonian \hat{H}_{eff} in Eq. (7) of the main text also possesses this spin SU(2) symmetry, no matter whether l is even or odd. This can also be verified directly by checking $[\hat{H}_{\text{eff}}, \hat{S}_\alpha] = 0$ for any $\alpha = x, y, z$. The spin-rotational symmetry hence allows us to automatically get a spin-balanced system without any additional magnetic field.

However, regarding the charge SU(2) symmetry, the time-dependent Hamiltonian lacks it for the appearance of the time-dependent on-site energy term [the last term in Eq. (4) of the main text]. As a result we do not expect the SO(4) symmetry in general. Nevertheless, it emerges in the effective Hamiltonian with l even. We introduce the charge SU(2) as follows [25]:

$$\hat{L}_z = -\frac{1}{2} \sum_i \hat{c}_{i\uparrow}^\dagger \hat{c}_{i\uparrow} + \hat{c}_{i\downarrow}^\dagger \hat{c}_{i\downarrow} + \frac{1}{2}N, \quad (\text{A3})$$

$$\hat{L}_+ = \sum_i (-1)^i \hat{c}_{i\uparrow} \hat{c}_{i\downarrow} = \sum_i \exp(i\mathbf{Q} \cdot \mathbf{x}_i) \hat{c}_{i\uparrow} \hat{c}_{i\downarrow}, \quad (\text{A4})$$

where $\mathbf{Q} = (\pi, \pi)$, N is the total number of lattice sites hereafter, and

$$\hat{L}_- = \hat{L}_+^\dagger, \quad \hat{L}_x = \frac{\hat{L}_+ + \hat{L}_-}{2}, \quad \hat{L}_y = \frac{\hat{L}_- - \hat{L}_+}{2i}. \quad (\text{A5})$$

$\{\hat{L}_z, \hat{L}_x, \hat{L}_y\}$ forms an SU(2) algebra. It can be verified straightforwardly that the effective Hamiltonian \hat{H}_{eff} with l even commutes with all these generators. This fact can also be seen from the following transformation:

$$\hat{P} : \hat{c}_{i\uparrow} \rightarrow (-1)^i \hat{c}_{i\uparrow}^\dagger,$$

which maps \hat{H}_{eff} with l even for interaction $+\tilde{U}$ to the same class but of effective interaction $-\tilde{U}$, exchanging the role played by $\{L_i\}$ and $\{S_i\}$. As a result, the spin SU(2) invariance for a model with $-\tilde{U}$ indicates the charge SU(2) symmetry for $+\tilde{U}$ and vice versa. In addition, this transformation also implies the phase diagram should be symmetric under $+\tilde{U} \leftrightarrow -\tilde{U}$ together with the interchange of charge and spin order. However, in the l odd cases, this mapping fails because of the additional minus sign in $\hat{d}_{i\sigma}$.

Particle-hole symmetry. The half-filled effective Hamiltonian \hat{H}_{eff} holds particle-hole symmetry no matter whether l is even or odd. (i) When l is even, define particle-hole transformation $\hat{C} : \hat{c}_{i\sigma} \rightarrow (-1)^i \hat{c}_{i\sigma}^\dagger$. The Hamiltonian is invariant under \hat{C} . $[\hat{C}, \hat{H}_{\text{eff}}] = 0$. (ii) When l is odd, we further define the bipartite transformation \hat{S} , which switches the A/B sublattices. Then the Hamiltonian is invariant under the combination of \hat{C} and \hat{S} : $[\hat{C}\hat{S}, \hat{H}_{\text{eff}}] = 0$. This symmetry allow us to fix chemical potential to $\mu = 0$ during the mean-field calculation at a half-filling situation.

APPENDIX B: MEAN-FIELD TREATMENT

In this section we establish the mean-field theory adopted in this work. As explained in the main text, assuming no canted order, we can consider only the charge-density-wave (CDW) order and spin-density-wave (SDW) order in the z direction because of the SO(4) symmetry. We focus on the half-filled spin-balanced system, in which case the total charge density and total magnetic momentum is given by

$$\langle \hat{n} \rangle = 1, \quad \langle \hat{S} \rangle = 0. \quad (\text{B1})$$

Path-integral approach. Here we provide a derivation of the mean-field Hamiltonian Eq. (B14) via a path-integral approach. In the path-integral language, the real-time partition function of the system is given by

$$\mathcal{Z} = \int \mathcal{D}\psi D\bar{\psi} \exp\left(i \int dt L\right) \quad (\text{B2})$$

$$\begin{aligned} L = & \sum_{i,\sigma} i\bar{\psi}_{i\sigma} \partial_t \psi_{i\sigma} + \sum_{(i,j),\sigma} [J_0 a_{ij\sigma} (\bar{\psi}\psi) + J_1 b_{ij\sigma}^l (\bar{\psi}\psi)] \\ & \times \bar{\psi}_{i\sigma} \psi_{j\sigma} - \tilde{U} \sum_i \bar{\psi}_{i\uparrow} \psi_{i\uparrow} \bar{\psi}_{i\downarrow} \psi_{i\downarrow}. \end{aligned} \quad (\text{B3})$$

Here ψ corresponds to the fermionic field operators, and $a_{ij\sigma}$ and $b_{ij\sigma}^l$ are given by replacing the operators in $\hat{a}_{ij\sigma}$ and $\hat{b}_{ij\sigma}^l$ with fields. Since the effective Hamiltonian [Eq. (7) in the main text] contains six-fermion terms, the traditional decoupling based on Hubbard-Stratonovich transformation does not apply directly. However, an alternative way of decoupling based on the similar spirit of Hubbard-Stratonovich transformation should be adopted here. Specifically, by inserting a δ function, we directly introduce the auxiliary bosonic field:

$$\mathcal{Z} = \int \mathcal{D}\psi D\bar{\psi} Dn \prod_{i\sigma} \delta(n_{i,\sigma} - \bar{\psi}_{i,\sigma} \psi_{i,\sigma}) \exp\left(i \int dt L\right) \quad (\text{B4})$$

$$\begin{aligned} L = & \sum_{i,\sigma} i\bar{\psi}_{i\sigma} \partial_t \psi_{i\sigma} + \sum_{(i,j),\sigma} [J_0 a_{ij\sigma}(n) + J_1 b_{ij\sigma}^l(n)] \bar{\psi}_{i\sigma} \psi_{j\sigma} \\ & - \tilde{U} \sum_i n_{i\uparrow} n_{i\downarrow}. \end{aligned} \quad (\text{B5})$$

Thanks to the δ function inserted, one could replace all $\psi^\dagger \psi$ by n in the action. As an equivalence check, if we integrate out n fields first, we get our original action back. Now we

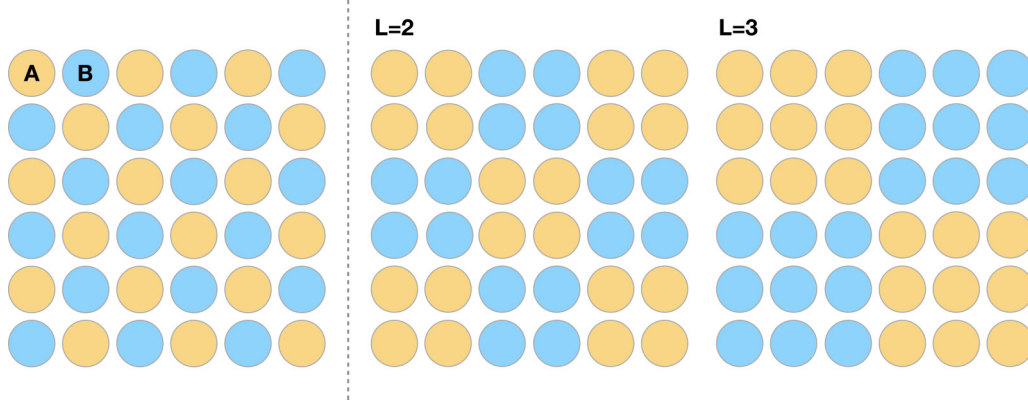


FIG. 6. Schematic of the two cases: (left panel) case 1, (right panel) typical examples of case 2 when $L = 2$ and $L = 3$, respectively, as labeled. Lattice sites of the same color have the same local particle density c_i and local spin density s_i .

introduce another field η to absorb the δ function into an integral:

$$Z = \int \mathcal{D}\psi D\bar{\psi} Dn D\eta \exp\left(i \int dt L\right) \quad (\text{B6})$$

$$L = \sum_{i,\sigma} i\bar{\psi}_{i\sigma} \partial_t \psi_{i\sigma} + \sum_{\langle i,j \rangle, \sigma} [J_0 a_{ij\bar{\sigma}}(n) + J_1 b'_{ij\bar{\sigma}}(n)] \bar{\psi}_{i\sigma} \psi_{j\sigma} - \tilde{U} \sum_i n_{i\uparrow} n_{i\downarrow} - \sum_{i\sigma} \eta_{i\sigma} (n_{i,\sigma} - \bar{\psi}_{i,\sigma} \psi_{i,\sigma}). \quad (\text{B7})$$

As a result, the fermion becomes quadratic. In general, one can integrate out all the fermions to get an effective action of wholly bosonic degrees of freedom, whereas the mean-field approximation says that all the bosonic fields will be replaced by their saddle-point solutions.

Mean-field Hamiltonian. By doing a Legendre transformation and replacing the fermion bilinears with its expectation values, we obtain the mean-field Hamiltonian

$$\hat{H} = \sum_{\langle i,j \rangle, \sigma} -[J_0 a_{ij\bar{\sigma}}(n) + J_1 b'_{ij\bar{\sigma}}(n)] \hat{\psi}_{i\sigma}^\dagger \hat{\psi}_{j\sigma} + \tilde{U} \sum_i n_{i\uparrow} n_{i\downarrow} + \sum_{i\sigma} \eta_{i\sigma} (n_{i,\sigma} - \hat{\psi}_{i,\sigma}^\dagger \hat{\psi}_{i,\sigma}), \quad (\text{B8})$$

where the following replacement is carried out:

$$\hat{a}_{ij\sigma} = (1 - \hat{n}_{i\sigma})(1 - \hat{n}_{j\sigma}) + \hat{n}_{i\sigma} \hat{n}_{j\sigma}, \quad (\text{B9})$$

$$\rightarrow (1 - n_{i\sigma})(1 - n_{j\sigma}) + n_{i\sigma} n_{j\sigma},$$

$$\hat{b}_{ij\sigma} = (-1)^j (1 - \hat{n}_{i\sigma}) \hat{n}_{j\sigma} + \hat{n}_{i\sigma} (1 - \hat{n}_{j\sigma}) \quad (\text{B10})$$

$$\rightarrow (-1)^j (1 - n_{i\sigma}) n_{j\sigma} + n_{i\sigma} (1 - n_{j\sigma}).$$

For the half-filled spin-balanced situation, we focus on the following two cases here: Notice that in a half-filled spin-balanced system, the local particle density can be expressed in terms of local charge density and local spin density as

$$n_{i\uparrow} = \frac{1}{2}(1 + c_i + s_i), \quad n_{i\downarrow} = \frac{1}{2}(1 + c_i - s_i), \quad (\text{B11})$$

where $\sum_i c_i = 0$ and $\sum_i s_i = 0$. The two cases are then

- (1) $c_i = (-1)^{i_x+i_y} c$, $s_i = (-1)^{i_x+i_y} s$
- (2) $c_i = (-1)^{\lceil i_x/L \rceil + \lceil i_y/L \rceil} c$, $s_i = (-1)^{\lceil i_x/L \rceil + \lceil i_y/L \rceil} s$

where c and s are CDW and SDW order parameters introduced, and $\lceil x \rceil$ denotes the ceiling function of x . Substituting these two expressions into the original mean-field Hamiltonian, Eq. (B8) will yield the mean-field Hamiltonian in each case.

Case 1. The first case is actually the (π, π) order, where the lattice is naturally divided into A/B sublattices and the unit cell of the lattice consists of two sites, with one from A and the other from B . The schematic is shown in Fig. 6 (left).

To be specific, we show here the work flow in the first case. By substitution,

$$n_A \equiv \langle \hat{n}_{i \in A} \rangle = 1 + c, \quad s_A \equiv \langle \hat{S}_{i \in A}^z \rangle = s/2, \quad (\text{B12})$$

$$n_B \equiv \langle \hat{n}_{i \in B} \rangle = 1 - c, \quad s_B \equiv \langle \hat{S}_{i \in B}^z \rangle = -s/2, \quad (\text{B13})$$

and the mean-field Hamiltonian is explicitly written as

$$\hat{H}_{\text{mf}} = \sum_{\langle i,j \rangle, \sigma} \{-J_0[(1 - n_{A\bar{\sigma}})(1 - n_{B\bar{\sigma}}) + n_{A\bar{\sigma}} n_{B\bar{\sigma}}] - J_1[(1 - n_{A\bar{\sigma}})n_{B\bar{\sigma}} + n_{A\bar{\sigma}}(1 - n_{B\bar{\sigma}})]\} \hat{c}_{i\sigma}^{A\dagger} \hat{c}_{j\sigma}^B + \text{H.c.} + \frac{\tilde{U}N}{2} (n_{A\uparrow} n_{A\downarrow} + n_{B\uparrow} n_{B\downarrow}) + \eta_c \left[c - \frac{(\hat{n}_{A\uparrow} + \hat{n}_{A\downarrow}) - (\hat{n}_{B\uparrow} + \hat{n}_{B\downarrow})}{2} \right] + \eta_s \left[s - \frac{(\hat{n}_{A\uparrow} - \hat{n}_{A\downarrow}) - (\hat{n}_{B\uparrow} - \hat{n}_{B\downarrow})}{2} \right], \quad (\text{B14})$$

where $\hat{c}_{i\sigma}^A$ ($\hat{c}_{i\sigma}^B$) are the annihilation operators of site i and spin σ on the A (B) sublattice, $\hat{n}_{\mu\sigma} = \frac{1}{N/2} \sum_{i \in \mu} \hat{n}_{i\sigma}$, $\mu = A$ or B , and $n_{\mu\sigma} = \langle \hat{n}_{\mu\sigma} \rangle$. Here η_c and η_s are Lagrangian multipliers of the CDW and SDW orders, respectively, which are also variational parameters to optimize the ground-state energy of \hat{H}_{mf} to get a mean-field solution.

After some substitution and simplification, the mean-field Hamiltonian in momentum space is written as

$$\begin{aligned} \hat{H}_{\text{mf}} = & \sum_{\mathbf{k}\sigma} -P_{\sigma}(c, s)Q(\mathbf{k})\hat{c}_{\mathbf{k}\sigma}^{A\dagger}\hat{c}_{\mathbf{k}\sigma}^B + \text{H.c.} + \frac{\tilde{U}N}{2}(1 + c^2 - s^2) \\ & + \eta_c \left[c - \frac{(\hat{n}_{A\uparrow} + \hat{n}_{A\downarrow}) - (\hat{n}_{B\uparrow} + \hat{n}_{B\downarrow})}{2} \right] \\ & + \eta_s \left[s - \frac{(\hat{n}_{A\uparrow} - \hat{n}_{A\downarrow}) - (\hat{n}_{B\uparrow} - \hat{n}_{B\downarrow})}{2} \right], \end{aligned} \quad (\text{B15})$$

where $\hat{c}_{\mathbf{k}\sigma}^A$ ($\hat{c}_{\mathbf{k}\sigma}^B$) are the annihilation operators on the A (B) sublattice of quasimomentum \mathbf{k} and spin σ , $Q(\mathbf{k}) = \sum_i \exp(i\mathbf{k} \cdot \mathbf{d}_i)$, $\{\mathbf{d}_i\}$ are the lattice vectors, and

$$P_{\uparrow}(c, s) = \frac{J_0}{2}[1 - (c - s)^2] + \frac{J_1}{2}[1 + (c - s)^2], \quad (\text{B16})$$

$$P_{\downarrow}(c, s) = \frac{J_0}{2}[1 - (c + s)^2] + \frac{J_1}{2}[1 + (c + s)^2]. \quad (\text{B17})$$

The summation of \mathbf{k} in Eq. (B15) is over the first Brillouin zone. Minimizing the energy for all parameters $\{c, s, \eta_c, \eta_s\}$

yields a set of mean-field equations that is solved by numerical iteration in this work.

Case 2. The second case actually includes a series of circumstances of L being 2, 3, 4, \dots , ∞ . Typical examples of $L = 2$ and $L = 3$ are shown in the right panel of Fig. 6. In this case, for each independent L , doing a similar substitution as above and solving the optimization problem in a numerical way returns us to a set of self-consistent mean-field solutions in each L . The ground state should be the one with the lowest ground-state energy.

Figures 2, 3, 4, and 5 in the main text are based on the mean-field numerics of the above two cases.

Check the formulation for $J_0 = J_1$. Finally, we explain why our mean-field theory reduces to a traditional one appearing in common textbooks, e.g., [38]. In fact, the P_{σ} in this case is just a constant with no c and s dependence. Thus the variation of c and s yields

$$\eta_c = -\tilde{U}Nc, \quad \eta_s = \tilde{U}Ns. \quad (\text{B18})$$

Using this relation, we see that the mean-field Hamiltonian reduces to a familiar one that appears in textbooks [38].

-
- [1] E. Haller, J. Hudson, A. Kelly, D. A. Cotta, B. Peaudecerf, G. D. Bruce, and S. Kuhr, Single-atom imaging of fermions in a quantum-gas microscope, *Nat. Phys.* **11**, 738 (2015).
- [2] L. W. Cheuk, M. A. Nichols, M. Okan, T. Gersdorf, V. V. Ramasesh, W. S. Bakr, T. Lompe, and M. W. Zwierlein, Quantum-Gas Microscope for Fermionic Atoms, *Phys. Rev. Lett.* **114**, 193001 (2015).
- [3] G. J. A. Edge, R. Anderson, D. Jervis, D. C. McKay, R. Day, S. Trotzky, and J. H. Thywissen, Imaging and addressing of individual fermionic atoms in an optical lattice, *Phys. Rev. A* **92**, 063406 (2015).
- [4] A. Omran, M. Boll, T. A. Hilker, K. Kleinlein, G. Salomon, I. Bloch, and C. Gross, Microscopic Observation of Pauli Blocking in Degenerate Fermionic Lattice Gases, *Phys. Rev. Lett.* **115**, 263001 (2015).
- [5] D. Greif, M. F. Parsons, A. Mazurenko, C. S. Chiu, S. Blatt, F. Huber, G. Ji, and M. Greiner, Site-resolved imaging of a fermionic Mott insulator, *Science* **351**, 953 (2016).
- [6] L. W. Cheuk, M. A. Nichols, K. R. Lawrence, M. Okan, H. Zhang, and M. W. Zwierlein, Observation of 2D Fermionic Mott Insulators of 40K with Single-Site Resolution, *Phys. Rev. Lett.* **116**, 235301 (2016).
- [7] M. F. Parsons, A. Mazurenko, C. S. Chiu, G. Ji, D. Greif, and M. Greiner, Site-resolved measurement of the spin-correlation function in the Fermi-Hubbard model, *Science* **353**, 1253 (2016).
- [8] M. Boll, T. A. Hilker, G. Salomon, A. Omran, J. Nespolo, L. Pollet, I. Bloch, and C. Gross, Spin- and density-resolved microscopy of antiferromagnetic correlations in Fermi-Hubbard chains, *Science* **353**, 1257 (2016).
- [9] L. W. Cheuk, M. A. Nichols, K. R. Lawrence, M. Okan, H. Zhang, E. Khatami, N. Trivedi, T. Paiva, M. Rigol, and M. W. Zwierlein, Observation of spatial charge and spin correlations in the 2D Fermi-Hubbard model, *Science* **353**, 1260 (2016).
- [10] T. A. Hilker, G. Salomon, F. Grusdt, A. Omran, M. Boll, E. Demler, I. Bloch, and C. Gross, Revealing hidden antiferromagnetic correlations in doped Hubbard chains via string correlators, *Science* **357**, 484 (2017).
- [11] G. Salomon, J. Koepsell, J. Vijayan, T. A. Hilker, J. Nespolo, L. Pollet, I. Bloch, and C. Gross, Direct observation of incommensurate magnetism in Hubbard chains, *Nature* **565**, 56 (2019).
- [12] P. T. Brown, D. Mitra, E. Guardado-Sanchez, P. Schaub, S. S. Kondov, E. Khatami, T. Paiva, N. Trivedi, D. A. Huse, and W. S. Bakr, Spin-imbalance in a 2D Fermi-Hubbard system, *Science* **357**, 1385 (2017).
- [13] D. Mitra, P. T. Brown, E. Guardado-Sanchez, S. S. Kondov, T. Devakul, D. A. Huse, P. Schaub, and W. S. Bakr, Quantum gas microscopy of an attractive Fermi-Hubbard system, *Nat. Phys.* **14**, 173 (2018).
- [14] A. Mazurenko, C. S. Chiu, G. Ji, M. F. Parsons, M. Kanasz-Nagy, R. Schmidt, F. Grusdt, E. Demler, D. Greif, and M. Greiner, A cold-atom Fermi-Hubbard antiferromagnet, *Nature (London)* **545**, 462 (2017).
- [15] R. Anderson, F. Wang, P. Xu, V. Venu, S. Trotzky, F. Chevy, and J. H. Thywissen, Conductivity Spectrum of Ultracold Atoms in an Optical Lattice, *Phys. Rev. Lett.* **122**, 153602 (2019).
- [16] M. A. Nichols, L. W. Cheuk, M. Okan, T. R. Hartke, E. Mendez, T. Senthil, E. Khatami, H. Zhang, and M. W. Zwierlein, Spin Transport in a Mott Insulator of Ultracold Fermions, *Science* **363**, 383 (2019).
- [17] P. T. Brown, D. Mitra, E. Guardado-Sanchez, R. Nourafkan, A. Reymbaut, S. Bergeron, A.-M. S. Tremblay, J. Kokalj, D. A. Huse, P. Schaub, and W. S. Bakr, Bad metallic transport in a cold atom Fermi-Hubbard system, *Science* **363**, 379 (2019).
- [18] M. Bukov, M. Kolodrubetz, and A. Polkovnikov, Schrieffer-Wolff Transformation for Periodically Driven Systems: Strongly Correlated Systems with Artificial Gauge Fields, *Phys. Rev. Lett.* **116**, 125301 (2016).

- [19] A. P. Itin and M. I. Katsnelson, Effective Hamiltonians for Rapidly Driven Many-Body Lattice Systems: Induced Exchange Interactions and Density-Dependent Hoppings, *Phys. Rev. Lett.* **115**, 075301 (2015).
- [20] F. Görg, M. Messer, K. Sandholzer, G. Jotzu, R. Desbuquois, and T. Esslinger, Enhancement and sign change of magnetic correlations in a driven quantum many-body system, *Nature (London)* **553**, 481 (2018).
- [21] W. Xu, W. Morong, H.-Y. Hui, V. W. Scarola, B. DeMarco, Correlated spin-flip tunneling in a Fermi lattice gas, *Phys. Rev. A* **98**, 023623 (2018).
- [22] R. Shankar, *Principles of Quantum Mechanics* (Springer, New York, 1994).
- [23] A. Eckardt and E. Anisimovas, High-frequency approximation for periodically driven quantum systems from a Floquet-space perspective, *New J. Phys.* **17**, 093039 (2015).
- [24] A. Eckardt, Colloquium: Atomic quantum gases in periodically driven optical lattices, *Rev. Mod. Phys.* **89**, 011004 (2017).
- [25] C. N. Yang and S. C. Zhang, SO_4 symmetry in a Hubbard model, *Mod. Phys. Lett. B* **4**, 759 (1990).
- [26] Appendix A proves the $SO(4)$ symmetry of the effective Hamiltonian for even l , and Appendix B describes the mean-field theory.
- [27] N. Nagaosa, *Quantum Field Theory in Condensed Matter Physics* (Springer, New York, 1999).
- [28] R. Strack and D. Vollhardt, Hubbard Model with Nearest-Neighbor and Bond-Charge Interaction: Exact Ground-State Solution in a Wide Range of Parameters, *Phys. Rev. Lett.* **70**, 2637 (1993).
- [29] L. Arrachea and A. A. Aligia, Exact Solution of a Hubbard Chain with Bond-Charge Interaction, *Phys. Rev. Lett.* **73**, 2240 (1994).
- [30] L. Arrachea, A. A. Aligia, and E. Gagliano, Anomalous Flux Quantization in a Hubbard Ring with Correlated Hopping, *Phys. Rev. Lett.* **76**, 4396 (1996).
- [31] A. A. Aligia, Liliana Arrachea, and E. R. Gagliano, Phase diagram of an extended Hubbard model with correlated hopping at half fillings, *Phys. Rev. B* **51**, 13774 (1995).
- [32] M. Di Liberto, C. E. Creffield, G. I. Japaridze, and C. Morais Smith, Quantum simulation of correlated-hopping models with fermions in optical lattices, *Phys. Rev. A* **89**, 013624 (2014).
- [33] G. I. Japaridze and A. P. Kampf, Weak-coupling phase diagram of the extended Hubbard model with correlated-hopping interaction, *Phys. Rev. B* **59**, 12822 (1999).
- [34] G. Japaridze and E. Muller-Hartmann, Electrons with correlated hopping interaction in one dimension, *Ann. Phys.* **3**, 163 (1994).
- [35] A. A. Aligia and Liliana Arrachea, Triplet superconductivity in quasi-one-dimensional systems, *Phys. Rev. B* **60**, 15332 (1999).
- [36] L. Arrachea, A. A. Aligia, E. Gagliano, K. Hallberg, and C. Balseiro, Superconducting correlations in Hubbard chains with correlated hopping, *Phys. Rev. B* **50**, 16044 (1994).
- [37] M. Messer, K. Sandholzer, F. Gorg, J. Minguzzi, R. Desbuquois, and T. Esslinger, Floquet Dynamics in Driven Fermi-Hubbard Systems, *Phys. Rev. Lett.* **121**, 233603 (2018).
- [38] A. Altland and B. D. Simons, *Condensed Matter Field Theory*, 2nd ed. (Cambridge University Press, Cambridge, England, 2010).